International Journal of Engineering Sciences & Research Technology

(A Peer Reviewed Online Journal)
Impact Factor: 5.164

IJESRT

Chief Editor

Dr. J.B. Helonde

Executive Editor

Mr. Somil Mayur Shah

IJESRT

INTERNATIONAL JOURNAL OF ENGINEERING SCIENCES & RESEARCH TECHNOLOGY
DESIGN AND EXPERIMENTAL STUDY OF ARM-TYPE CABLE TUNNEL INSPECTION TRACKED ROBOT

Shufeng TANG*, Yue YU, Zirui GUO, Wenzhi ZHANG, Yigang DU
* School of mechanical engineering, Inner Mongolia University of Technology, Hohhot 010051, China   tangshufeng@imut.edu.cn

ABSTRACT
For solving the safety hazards and inspection safety problems in the long-term operation of cable tunnel transmission, on the investigation of the working environment and requirements, an arm-type cable tunnel inspection robot was designed. Making the kinematics analysis for this robot, a robot-to-barrier method is proposed and the obstacle path is planned. And then the kinematics and dynamics analysis of the climbing process were carried out, and calculate the theoretical value of the biggest obstacle that the robot can cross. By establishing a robot simulation model to simulate the climbing steps and climbing process of the robot. Finally, a variety of environmental experiments were conducted for the inspection robots, and demonstration applications were carried out in actual cable tunnels. The test and demonstration application results show that the robot has smooth and flexible movement, strong environmental adaptability, the ability for reliable communication and convenient operation so that it can meet the requirements of inspection operations.

KEYWORDS: Arm and track, Electric cable tunnel, Mobile robots, Inspection tours, Obstacle negotiation.

1.   INTRODUCTION
In order to reduce the impact of natural disasters on transmission lines, to improve the appearance of the city, to avoid interference between overhead cables and ground buildings, and to take the convenience of cable expansion and maintenance into account, more and more cables are used to transport underground[1-2] . With the running time, cable aging, corrosion and other phenomena will inevitably occur. If the cable runs in an unhealthy condition for a long time, it will inevitably cause transmission failure, affecting production and living electricity, and causing huge losses to the social economy[3]. Although the cable is equipped with detection and alarm facilities, its detection range is limited, and there are observation dead angles, which can only passively play an auxiliary observation role, and cannot actively discover some potential hidden dangers in time. And therefore, it is urgent to increase the frequency of live inspections of underground transmission lines, identify potential safety hazards in time, and improve transmission safety and reliability.

The internal environment of the cable tunnel is complicated. In the process of inspection, the robot will inevitably encounter obstacles such as water accumulation, gravel, gully and steps. The ordinary tracked robot is difficult to adapt to the complicated terrain inside the cable tunnel. The composite tracked mobile robot has a deformable tracked structure, which can climb a variety of obstacles, greatly improving the adaptability to complex terrain, and is suitable for the inspection of cable tunnels. In recent years, many research institutes at home and abroad have developed a variety of composite tracked robot which have certain reference significance for the development of cable tunnel inspection robots. The main structural forms include: 1. Multi-track composite. There are two or four adjustable angled swing arm-assisted robots for obstacle crossing and climbing before and after the robot. Currently, research institutions include Tohoku University in Japan and Sorbonne University in France. There are Beijing Institute of Technology, Shanghai Jiaotong University, Shanghai University, Xi'an University of Electronic Science and Technology etc. [5-13]. 2, Deformable crawler type. The robot's track mechanism can be deformed according to the actual work needs, greatly increasing the robot's ability to climb and overcome obstacles. The current research institutions include Beijing Institute of Technology, Shenyang Electric Power Research Institute and Shenyang Institute of Automation [14-17]. 3, Wheel and wheel composite. The robot can be freely switched between the wheeled and tracked type traveling mechanism, and has both the high speed of the wheeled traveling mechanism and the high passability of the tracked type traveling mechanism. The research

institutes include Beijing Institute of Technology, National University of Defense Technology, and Hebei University of Technology [18-22]. 4, The leg and the combined robot. The robot is equipped with mechanical legs. The mechanical legs can not only support the robot during the obstacle crossing process, but also can be used as an operating arm for various operations. The research institutes include Japan Northeastern Polytechnical University and Shanghai Jiaotong University.[23 -25].

At present, the traditional obstacle-crossing mode of crawler robots is mainly divided into two types: the crawler-type walking mechanism directly overcomes the obstacle and the swing-arm-track composite obstacle. Both the wheeled composite and the deformable crawler are direct obstacle-crossing mechanisms. The principle is that the inclination of the robot body design is over the obstacle and the structure is simple. However, the centre of gravity of the robot is high and when it is over a high obstacle, it is prone to overturning; The multi-track composite and the leg-and-shoulder combination are all complex obstacles, and the robot with the composite obstacle-crossing mechanism has a lower centre of gravity. Although the structure is complicated, it relies on the support of the swing arm to effectively climb higher obstacles.

In this paper, a boom-and-compartment mobile robot structure which is different from the above-mentioned robot is designed. The robot is equipped with the double-swing arm structure used to assist the robot to overcome obstacles. Through planning the reverse obstacle path of the robot ,the kinematics and power of the robot climbing the step as well as the analysis and simulation and experiments are carried out in order to verify the stability and reliability of the robot's obstacle crossing process

2. THE STRUCTURE DESIGN OF THE INSPECTION ROBOT

Subheading

According to the structural characteristics of the cable tunnel, the task of the inspection work and the design requirements of the mechanism, a patrol robot which is very suitable for small and medium-sized cable tunnels is finally designed, whose three-dimensional model is shown in Figure.1(a). The robot is mainly composed of a Mobile parts of robots, a swing arm obstacle avoidance mechanism and a controllable Pan-title. The swing arm obstacle mechanism is composed of a driving device (including a motor, a speed reducer, an encoder), a transmission gear, a transmission shaft, a swing arm, and so on. And its structural diagram is shown in Figure 1(b).

(a)   (b)
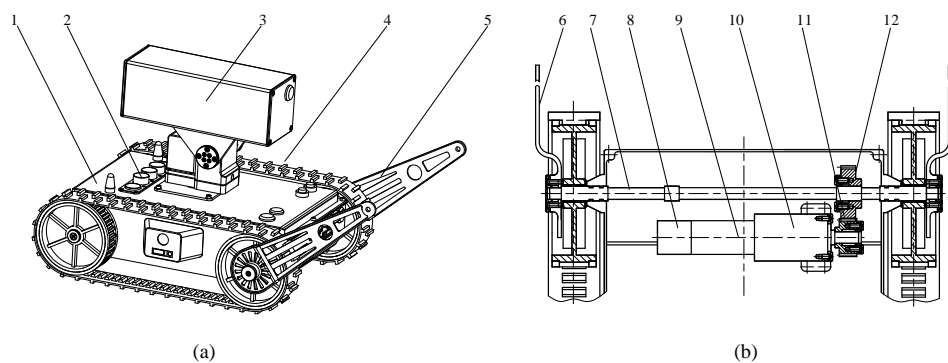
1. Mobile parts of robots 2. Sensing system 3. Pan-title 4. Walking mechanism 5. Swinging arm 6. Swing arm 7. Transmission shaft 8. Encoder 9. Motor 10.Speed reducer 11. Drive Gear 12. Driven Gear

Figure 1. Three-dimensional model of robot

3. OBSTACLE PATH PLANNING AND K INEMATICS ANALYSIS

3.1 The Path Planning of Climbing

In order to adapt to the unknown environment encountered during the inspection, a simple swing arm mechanism is designed, and the three motors are coordinated with each other to control the robot to complete the obstacle smoothly. In order to ensure the orderly completion of the obstacle crossing process of the robot, it is necessary to plan the obstacle crossing path. The first step is used as an obstacle for the robot to climb.

The robot climbs the first step in both forward and reverse directions. Because the center of gravity of the inspection robot designed by this project is ahead of the front, in order to ensure the smooth transition of the robot, the reverse climbing mode is selected, as shown in Figure 2.
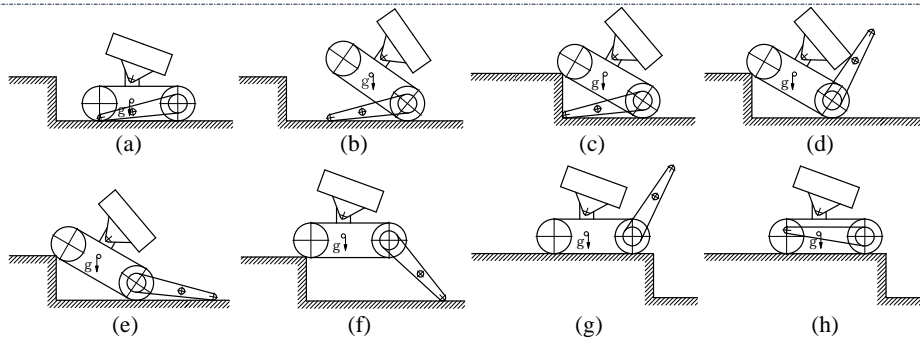
Figure 2．Reverse climbing steps

When the robot encounters a step, the swing arm drives the motor to work, and controls the swing arm to rotate, so that the robot body rotates around the driven pulley by a certain angle. Under the traction of the pulley drive motor, the whole body moves forward, so that the tracks are placed on the outer corner line of the step, and then the swing arm rotates to support the robot body, and the center of mass is moved upwards. When the robot is running to the horizontal position, the pulley motor drives the track to complete the process of climbing the steps.

3.2 Kinematics Analysis of Climbing Steps
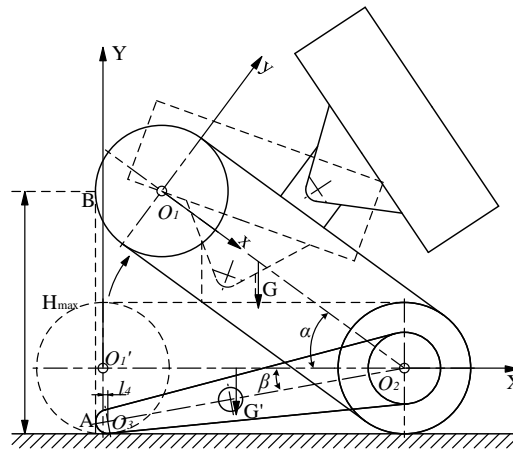
Figure3．Robot Pendulum state diagram

As shown in Figure 3, the coordinate system $XO_1'Y$ and XO_1Y are respectively established as the coordinate origins before and after the lifting of the front body of the robot body mechanism, and the distance between the front and rear pulleys of the robot is l_0, and the front and rear centers of the swing arm are l_1. The length of the pulley is R, the radius of the pulley is R, the thickness of the track is included, the radius of the end of the swing arm is r, and the width of the robot is d; The mass of the body part is m, and the coordinate of the center of mass G is $(1, h)$. When climbing a typical obstacle (taking the first step as an example), the two swing arms need to be synchronously oscillated. Since the quality of the swing arm is relatively light relative to the overall quality, the influence on the overall center of mass change is small. To simplify the model, the quality is neglected in the analysis. Therefore, the centroid G of the body part is the centroid of the robot.

It can be seen from the motion planning of the obstacle crossing process that the robot uses the reverse climbing step to complete the obstacle. In order to achieve the smooth realization of the whole process, it is first necessary to ensure that the robot body part can rotate with the end of the swing arm as the fulcrum and rotate around O_2, so that the front wheel O_1 of the robot is lifted. The angle between O_1O_2 and O_2O_3 and the horizontal plane during the lifting of the front wheel of the robot is $\alpha(0 \le \alpha \le \pi)$ and β, respectively, where α is the depression angle of the robot body and $\beta = \arcsin[(R-r)/l_1]$ is a fixed value. The coordinates of the centroid of the robot under the coordinate system $XO_1'Y$ are:

$$\begin{cases} X_G = l_0 + h\sin\alpha - (l_0 - l)\cos\alpha \\ Y_G = h\cos\alpha + (l_0 - l)\sin\alpha \end{cases} \qquad \text{(i)}$$

Simplified:

$$(X_G - l_0)^2 + Y_G^2 = h^2 + (l_0 - l)^2 \qquad \text{(ii)}$$

It can be seen that in the $XO_1'Y$ coordinate system, during the lifting process of the front wheel of the robot, the robot's centroid trajectory is a circle with $(l_0, 0)$ as the center and as the radius.

In order to avoid the overturning phenomenon during the climbing process, the robot body elevation angle $\alpha \in (0, \pi/2)$, then

$$\frac{dX_G}{d\alpha} = h\cos\alpha + (l_0 - l)\sin\alpha > 0 \qquad \text{(iii)}$$

That is, the abscissa $X_G(\alpha)$ of the centroid increases as α increases, so as long as it satisfies:

$$\begin{cases} X_G(\alpha = 0) = l_0 + h\sin\alpha \\ -(l_0 - l)\cos\alpha \big|_{\alpha=0} = l > l_4 \end{cases} \qquad \text{(iv)}$$

Among them $l_4 = l_0 - l_1\cos\beta$, that is the vertical distance from the O_3 to the Y -axis, the robot body has the swing arm end O_3 as a fulcrum, and the robot drive pulley O_1 can be lifted around the driven pulley O_2 . If $X_G(\alpha = 0) < l_4$,the robot driven pulley O_2 is lifted around the drive pulley O_1, which is an effect we do not want. After the robot drive pulley O_1 is lifted up, as α gradually increases, the centroid shifts in the positive direction of the X -axis. When $X_G = l_0$, the limit position is reached, and the robot just does not overturn, so the critical value α_1 of α can be found:

$$\alpha_1 = \arctan\frac{l_0 - l}{h} \qquad \text{(v)}$$

It can be seen from the analysis of Fig. 3 that after the robot body is swung, only when the projection of the synchronous track in the horizontal plane is greater than or equal to the projection of the swing arm in the horizontal plane, the robot track can be placed on the step. When the two are equal, the maximum allowable angle α_2 of the robot can be found.

$$\alpha_2 = \arccos\frac{l_1\cos\beta + r - R}{l_0} \qquad \text{(vi)}$$

In summary, when the robot elevation angle α is taken $\alpha_{\min} = \min(\alpha_1, \alpha_2)$, the robot track can rest on the outer corner of the step, and the step height $H_S = R + l_0\sin\alpha_{\min}$ at this time is the maximum height that the robot can climb. According to the design characteristics of the swing arm mechanism in this paper, the robot can theoretically cross the step with the maximum height $(H_{\max})$ of 150mm. In practice, the robot can effectively meet the requirements of obstacles with a height of 100mm.

4.   4. DYNAMIC ANALYSIS OF ROBOT

4.1 Dynamic Analysis of Robot Climbing

When the robot climbs the slope, the force is shown in Figure 4. The direction of the robot (ie, parallel to the slope) is the X-axis, and the vertical slope is the Y-axis. The Cartesian coordinate system XOY is established. Among them, G is the robot gravity, F is the driving force, F_N is the slope support force, F_f is the friction force, and the robot mass is m, and the slope gradient is θ , which is obtained by Newton's second law:

$$\begin{cases} \sum F_X = F - F_f - G\sin\theta = ma \\ \sum F_Y = F_N - G\cos\theta = 0 \end{cases} \qquad \text{(vii)}$$

Where a is the robot's travel acceleration, and $\sum F_X$ and $\sum F_Y$ are the sum of the forces acting on the X and Y axes, respectively.
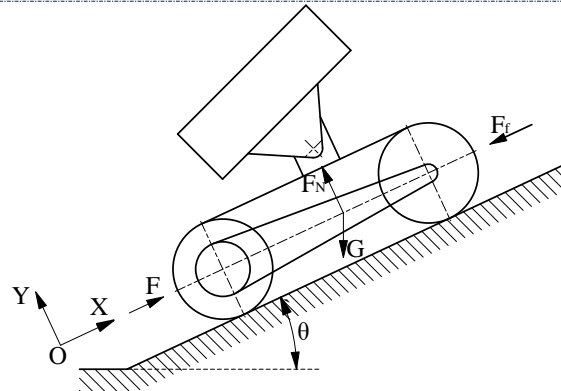
Figure 4. The sketch of robotic force when climbing

It can be known from equation (vii) that when $\sum_{F_X} = 0$, $a = 0$, the robot makes a uniform linear motion; when $\sum_{F_X} > 0$, $a > 0$, the robot accelerates uphill; when $\sum_{F_X} < 0$, $a < 0$, the robot accelerates downhill. In addition, the movement of the robot on the slope also overcomes the friction of the track, then

$$F_f = \mu F_N \qquad \text{(viii)}$$

Among the equation, a is the sliding friction coefficient, and put (viii) into (vii), and simplification can be obtained:

$$F = G(f_1 \cos\theta + \sin\theta) + ma \qquad \text{(ix)}$$

According to the robot design requirements, the slope slope $\theta \in (0, 30^o)$, after consulting the relevant data, the friction coefficient $\mu \in (0.6, 0.8)$ of the rubber track and the ground, so when the robot performs uniform motion (ie $a = 0$) on the slope, the driving force F and the slope θ of the pulley motor are calculated. The relationship diagram is shown in Figure 5.
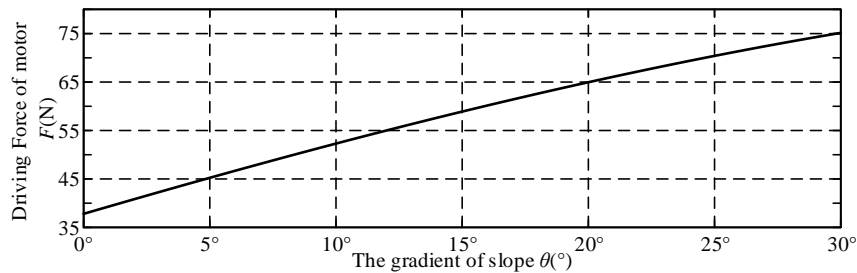
Figure 5. The relation graph between driving force of motor and gradient of slope

It can be seen from Figure 5. that under the condition that the friction coefficient μ is constant, the driving force F has a certain curve relationship with the slope gradient θ, and increases as θ increases. When the slope is $\theta = 30^o$, the driving force F reaches the maximum, that is: $F_{\max} = 75.14N$ (where μ takes 0.8), at which time the moment $T_{\max} = F_{\max}R = 4.14Nm$ is driven. According to the driving torque provided by the robot pulley drive motor:

$$T_D = n\eta_1 T_M i_1 \qquad \text{(x)}$$

Among the equation, n is the number of motors, T_{M1} is the rated torque of the pulley drive motor, i_1 is the transmission ratio of the output shaft of the pulley drive motor to the pulley shaft, and η_1 is the transmission efficiency of the pulley drive motor.

It can be obtained from Equation 10, $T_D = 5.89Nm > T_{\max}$, that is, the torque provided by the pulley drive motor is greater than the maximum torque required for the robot to walk or climb. Therefore, the selection of the robot pulley drive motor meets the requirements, and the robot can provide sufficient power for walking or climbing (slope $\theta < 30^o$).

4.2 Dynamic Analysis of Robot Climbing Boss

In the whole process of climbing the boss, the force analysis of the robot is mainly divided into two parts: one is the process of the swing arm touching the ground, the robot body is raised around the center O_2 of the rear wheel;

the other is that the front wheel of the robot is resting on the outer corner of the boss. On the upper side, the swing arm rotates in the opposite direction and touches the ground again, and the robot body is lifted to the horizontal position.
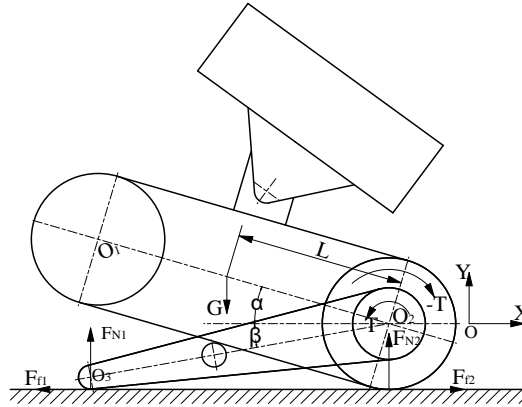
Figure 6. The first stress graph during crossing convex platform

First, when the swing arm touches the ground for the first time, the force of the robot is as shown in Figure.6. The horizontal direction is the X axis, and the vertical direction is the Y axis, and the Cartesian coordinate system XOY is established. Where T is the driving torque of the swing arm motor, F_{N1} and F_{N2}, F_{f1} and F_{f2} are the ground supporting force and friction force respectively received by the swing arm and the robot body, and L is the distance from the center of mass to the center O_2 of the rear wheel, and the remaining parameters are already in the front description.

The swing arm, the body and the robot are selected as the research objects respectively. If the robot body makes a uniform circular motion around the center O_2 of the rear wheel, it can be obtained according to Newton's second law:

$$\begin{cases} F_{f1} = F_{f2} \\ G = F_{N1} + F_{N2} \\ T = GL\cos\alpha + F_{f2}R \end{cases} \quad (xi)$$

Since the swing arm and the track also overcome the sliding friction on the ground, then

$$\begin{cases} F_{f1} = \mu_1 F_{N1} \\ F_{f2} = \mu_2 F_{N2} \end{cases} \quad (xii)$$

Among them, μ_1, μ_2 are the dynamic friction coefficient of the swing arm and the ground, the crawler belt and the ground respectively. After consulting relevant information, in general, $\mu_1 \in (0.15, 0.3)$, $\mu_2 \in (0.6, 0.8)$.

Substituting equation (xii) into equation (xi), and after simplification,

$$T = G(L\cos\alpha + \frac{\mu_1\mu_2}{\mu_1 + \mu_2}R) \quad (xiii)$$

According to the design requirements, the robot body elevation angle $\alpha \in (0, \pi/2)$, calculated the relationship between the swing arm motor driving torque T and the elevation angle α as shown in Figure 7.
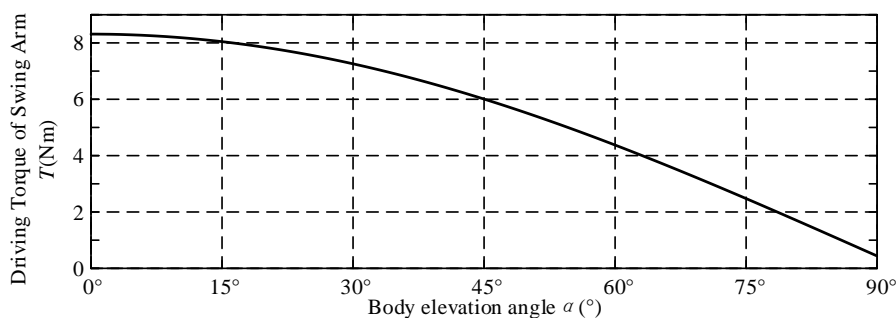
Figure 7. The relation graph between driving torque of swing arm and body elevation

RESEARCHERID

THOMSON REUTERS

[Tang* et al., 8(8): August, 2019]
IC™ Value: 3.00

ISSN: 2277-9655
Impact Factor: 5.164
CODEN: IJESS7

It can be seen from Figure7. that, in the case of μ_1 and μ_2, the driving torque of the swing arm motor is inversely proportional to the elevation angle of the robot body, that is, as the elevation angle α becomes larger, the moment f gradually decreases; When the robot body is just about to be lifted ($\alpha = 0^o$), the driving torque T is the largest, $T_{max} = 8.31Nm$ (take $\mu_1 = 0.15$, $\mu_2 = 0.8$). Due to the driving torque provided by the swing arm

$$T_{SA} = \eta_2 T_{电机2} i_2 \qquad (xiv)$$

Among them, $T_{电机2}$ is the rated torque of the swing arm motor, i_2 is the transmission ratio of the output shaft of the swing arm motor to the swing arm shaft, and η_2 is the transmission efficiency of the swing arm motor.

$T_{SA} = 11.9 Nm > T_{max}$ can be gained from the equation(xiv), so the swing arm motor can provide the torque required to lift the robot body.

And then, when the swing arm rotates in the opposite direction for the second time and lifts the robot body, the force is as shown in Figure 8. The horizontal direction is the X axis and the vertical direction is the Y axis, and the Cartesian coordinate system XOY is established. Among them, the elevation angle of the robot body is α, and α changes from α_0 (initial elevation angle) to 0 during the body lifting process, and the remaining parameters are known.
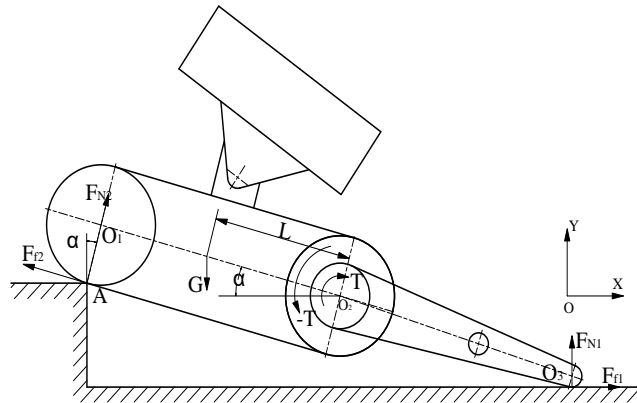
Figure 8. The second stress graph during crossing convex platform

From Figure 8., the swing arm, the body and the robot are selected as the research objects respectively, and it is assumed that the robot makes a counterclockwise uniform circular motion around the point A. In addition, after analysis, during the body lifting process, the swing arm slides to the right and then to the left, so there are three points at a certain time O_1, O_2 and O_3, which are connected to a straight line, that is, the swing arm slides to the right to the maximum position. The elevation angle of the robot body is α_1, according to Newton's second law:

When $\alpha_1 \le \alpha \le \alpha_0$, the swing arm slides to the right, then

$$\begin{cases} G = F_{N1} + F_{N2}\cos\alpha + F_{f2}\sin\alpha \\ F_{N2}\sin\alpha = F_{f2}\cos\alpha + F_{f1} \\ T + GL\cos\alpha + F_{f2}R = F_{N2}l_0 \end{cases} \qquad (xv)$$

When $0 \le \alpha < \alpha_1$, the swing arm slides to the left, then

$$\begin{cases} G = F_{N1} + F_{N2}\cos\alpha + F_{f2}\sin\alpha \\ F_{N2}\sin\alpha + F_{f1} = F_{f2}\cos\alpha \\ T + GL\cos\alpha + F_{f2}R = F_{N2}l_0 \end{cases} \qquad (xvi)$$

Simplified the equation (xv)and equation (xvi):

When $\alpha_1 \le \alpha \le \alpha_0$,

$$T = \frac{(l_0 - \mu_2 R)\mu_1 G}{(\mu_1\mu_2 + 1)\sin\alpha + (\mu_1 - \mu_2)\cos\alpha} - GL\cos\alpha \qquad (xvii)$$

When $0 \le \alpha \le \alpha_1$,

$$T = \frac{(l_0 - \mu_2 R)\mu_1 G}{(\mu_1\mu_2 - 1)\sin\alpha + (\mu_1 + \mu_2)\cos\alpha} - GL\cos\alpha \qquad \text{(xviii)}$$

According to the robot's obstacle-resistance performance requirement, the height of the boss is 100mm. After calculation, the initial elevation angle of the robot is $\alpha_0 = 22.5°$, and the elevation angle of O_1, O_2, O_3 is $\alpha_1 = 16.6°$. In addition, the parameters G, l_0, L, and R are known, and μ_1 and μ_2 are respectively 0.15 and 0.8, and the relationship between the driving torque T of the swing arm motor and the elevation angle α is calculated as shown in figure 9.
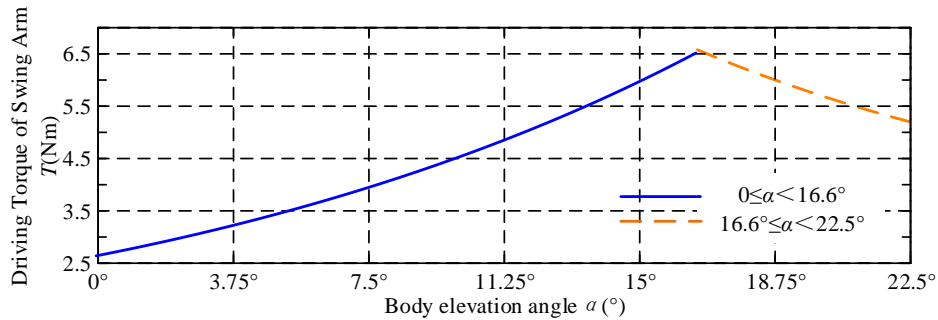
Figure 9 The relation graph between driving torque of swing arm and body elevation

The robot is placed on a boss with a height of 100mm. Under the condition of μ_1 and μ_2, when $0 \le \alpha < \alpha_1$, the driving torque of the swing arm is proportional to the elevation angle of the body. When $\alpha_1 \le \alpha \le \alpha_0$, the driving torque of the swing arm is inversely proportional to the elevation angle of the body. And $\alpha = \alpha_1$, the driving torque reaches the maximum, that is, $T_{max} = 6.57Nm < T_{SA}$, so the selection of the swing arm motor fully meets the requirements.

4.3 Simulation Experiment and Analysis Based on RecurDyn

In order to further verify the obstacle performance of the robot, the robot simulation model was established by using the *RecurDyn* secondary development function. The obstacle model is established according to the calculated maximum step and slope angle values, and the climbing steps as well as slope simulation experiments are carried out to verify the accuracy of the theoretical calculation value and at last to obtain the driving torque required by the robot during the obstacle crossing process.

4.3.1 Simulation and analysis of climbing robot climbing

First of all, for the actual working environment of the robot, two different road surfaces are set: hard soil road surface and sticky soil road surface, and 15° and 30° slopes are respectively arranged in the road surface; Then, add a motor drive to the pulley rotation pair to set the motor speed to 60deg/s. Finally, set the simulation time to 72 seconds and the number of steps to 300 steps. After the simulation calculation is completed, run and view the simulation results.

As shown in Figure 10 (a) ~ (d), the patrol robot climbs over the slope simulation process, and the torque of the single pulley drive motor changes with time as shown in Figure.11(a) and Figure.11(b)
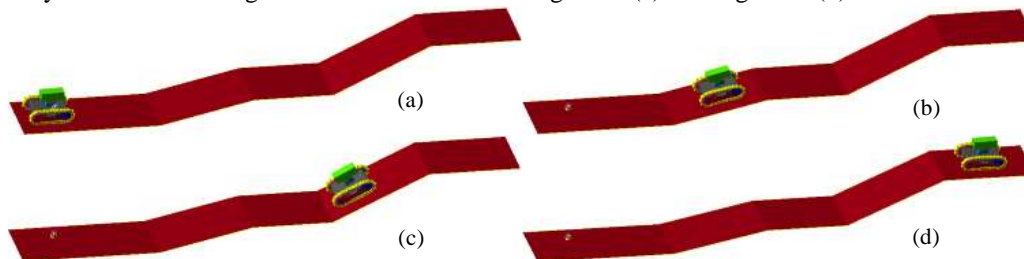
Figure 10. The simulation process diagram of the inspection robotic climbing

a.Hard soil road surface   b.Sticky soil road surface
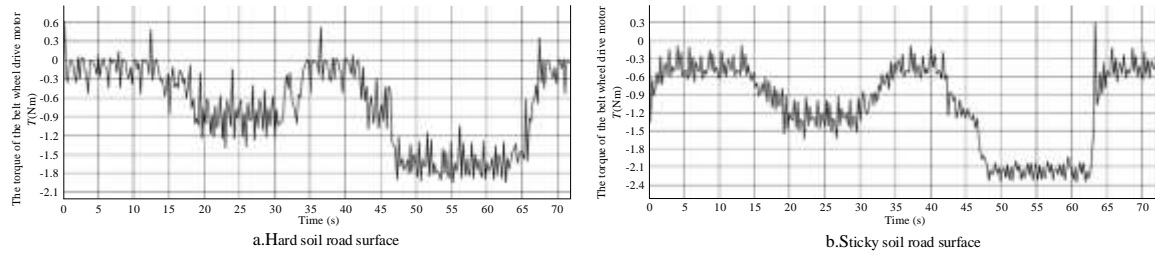
Figure 11. The torque of the belt wheel drive motor on different ground

From the relationship between the torque of a single pulley drive motor and the time difference between the two roads in Figure 11, it can be seen that the dynamic analysis results of the robot climbing are basically the same. And therefore, the motor selection meets the requirements of the inspection robot to climb the 30° slope.

4.3.2 Simulation and analysis of climbing robot climbing steps

According to the robot's obstacle performance requirements, a boss with a vertical height of 100 mm is established, and a hard road surface is selected as the simulation ground. Among them, the soil hardness is 0.219, the cohesive force is 4.14×10-3, the shear strength is 13, the shear deformation modulus is 25, the simulation time is set to 30 seconds, and the number of steps is 1000 steps. After the simulation calculation is completed, the simulation results can be observed and analyzed.

The simulation process of the patrol robot climbing the boss is shown in Figure.12(a)~(h), and the relationship between the torque of the swing arm and the pulley drive motor over time during the climbing process is shown in Figure.13(a) and Figure.13(b).

(a)   (b)   (c)   (d)

(e)   (f)   (g)   (h)
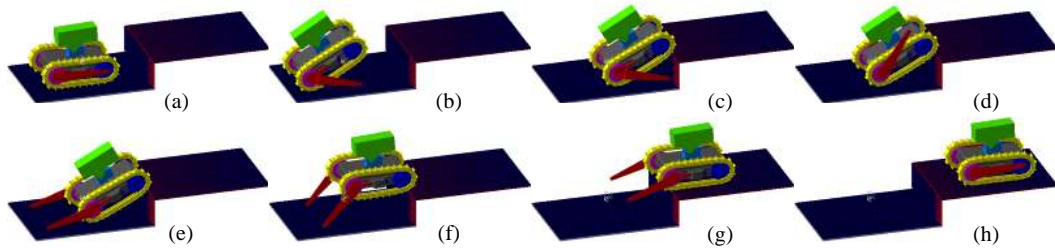
Figure12 The simulation process diagram of the inspection robotic crossing convex platform

a.Swing arm drive motor   b.Belt wheel drive motor
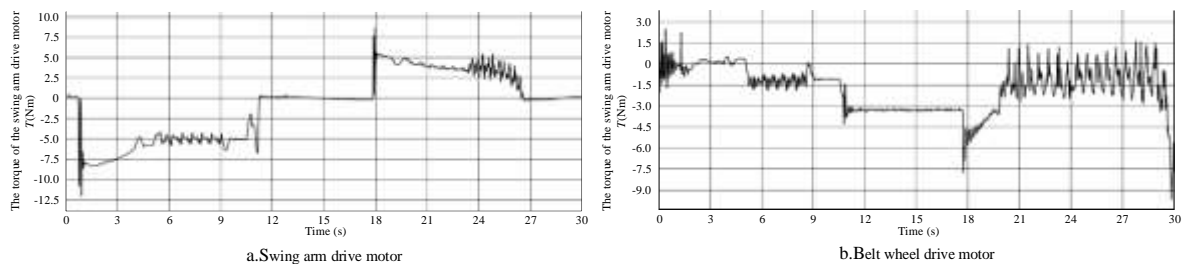
Figure 13. The torque of the drive motor

It can be seen from the relationship between the torque of the driving motor and the time when the robot climbs the boss in Figure.13 that the simulation analysis result of the robot climbing the boss is basically consistent with the dynamic analysis result. The required torque of the robot during the climbing step is lower than the maximum torque that the motor can provide. The selection of the swing arm drive motor and the pulley drive motor meets the requirements.

5.   TEST AND DEMONSTRATION APPLICATION OF INSPECTION ROBOT

After the successful development of the cable tunnel inspection robot, in order to further verify the rationality of the robot mechanism design and the reliability of the control system, it conducts tests and analysis on climbing , obstacles and communication. And carry out the demonstration application work in the actual cable tunnel.

5.1 Inspection robot test research

5.1.1 Hill climbing test

In the climbing test, a slope with a slope of about 25° is selected as the robot test object, and the robot can stably climb the 25° slope, as shown in Figure 14(a)~(f).

(a) (b) (c) (d) (e) (f)
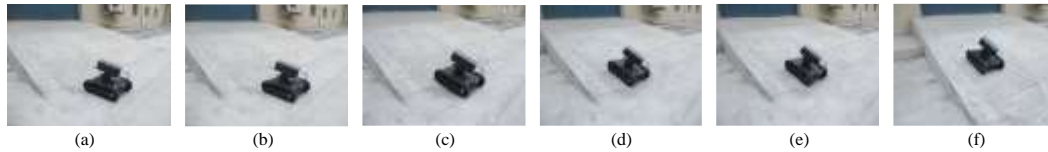
Figure 14. The climbing process of Inspection robot

5.1.2 Climbing boss test and analysis

Two small obstacles were selected as the robot's spanning obstacles in the small obstacle test. They are the boss with the vertical height of about 40mm and the car speed bump. The robot can stably cross small obstacles with a vertical height of 40mm, as shown in Figure 15.

(a) (b) (c) (d) (e) (f)

Figure 15. The process of inspection robot's climbing

5.2 Inspection robot demonstration application

In order to verify the actual application effect of the inspection robot, the demonstration application of the inspection robot was carried out in the actual cable tunnel, as shown in Figure 16.
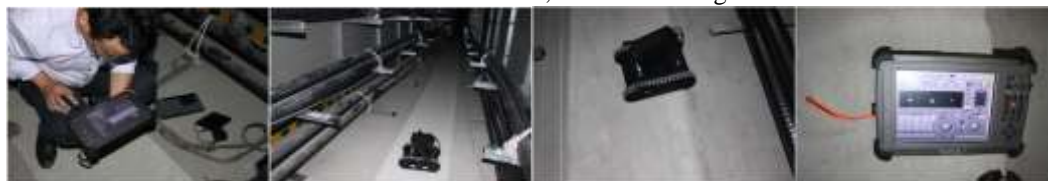
Figure 16. Debugging and application diagram of inspection robot in cable tunnel

Through the handheld operator, the environmental status and gas information in the tunnel can be seen. From the feedback information, it can be seen that the various gas information in the tunnel is within the safe range, there is no over-standard phenomenon, the cable running state is normal, and there is no over-temperature phenomenon, as shown in Figure 17.

Figure 17. Inspection robot returns the state information in the tunnel

6.   CONCLUSIONS

For the problem of power transmission safety in cable tunnels, after fully analyzing the actual environmental conditions of cable tunnels, a project that arm-type cable tunnel inspection tracked robot that can replace manual inspection is proposed. The overall integration of the robot is high and the structure is compact; the working mode of the combination of the arm and the arm can assist the robot to perform the obstacle crossing operation; the combination of software and hardware achieves a high degree of integration and information transmission of small computers, video images, infrared heat maps, multi-sensors and wireless communication, and effectively provides cable operation status for the staff. A way to overcome obstacles is proposed, and the obstacle path of the robot is planned. The kinematics analysis of the climbing process is carried out. At the same time, the robot control system

was developed, and the robot primary obstacle-crossed experiment and on-site inspection experiment were carried out. Experiments show that the robot is stable and flexible, with strong environmental adaptability, reliable communication and convenient operation, and meets the requirements of inspection of cable tunnels.

7. ACKNOWLEDGEMENTS

REFERENCES

[1] Lienert P, Sütterlin B, Siegrist M. Public acceptance of high-voltage power lines: The influence of information provision on undergrounding[J]. Energy Policy, 2018, 112:305-315.

[2] Liao Y, Sun T, Zhang L, et al. Power cable condition monitoring in a cable tunnel: Experience and inspiration[C]// International Conference on Condition Monitoring and Diagnosis. IEEE, 2016:594-597..

[3] Hu Yi, Liu Kai, Wu Tian, et al. [J].High Voltage Technology, 2014, 40 (11): 3491-3499.

[4] Endo D, Watanabe A, Nagatani K. Stair Climbing Control for 4-DOF Tracked Vehicle Based on Internal Sensors[J]. Journal of Robotics, 2017, 2017.

[5] Dong P, Wang X, Xing H, et al. Design and control of a tracked robot for search and rescue in nuclear power plant[C]. 2016 International Conference on Advanced Robotics and Mechatronics, ICARM 2016, August 18, 2016 - August 20, 2016, 2016: 330-335.

[6] Yanqiong F , Qiuxuan W , Yuhang Z . Study on climbing slope of wheel-track hybrid mobile robot[C]// International Conference on Mechatronics & Machine Vision in Practice. IEEE, 2017.

[7] Guo J, Shi J, Zhu W, et al. Approach to autonomous stair climbing for tracked robot[C]. 2017 IEEE International Conference on Unmanned Systems, ICUS 2017, October 27, 2017 - October 29, 2017, 2018: 182-186.

[8] Jun J-Y, Saut J-P, Benamar F. Pose estimation-based path planning for a tracked mobile robot traversing uneven terrains[J]. Robotics and Autonomous Systems, 2016, 75: 325-339.

[9] Luo J , Wu B , Pu H , et al. Boss-climbing capability analysis of tracked mobile robot with 6-DOF[C]// IEEE International Conference on Information & Automation. IEEE, 2015.

[10] Xie M, Wang C. Simulation study on the obstacle-surmounting of the 4 swing arms-6 tracked robot[C]. 15th International Conference on Ubiquitous Robots, UR 2018, June 27, 2018 - June 30, 2018, 2018: 926-928.

[11] Xiong P, Song A, Ji P, et al. Study on ability of a mobile tracked robot for stair-climbing based on static analysis[C]. 5th Annual IEEE International Conference on Cyber Technology in Automation, Control and Intelligent Systems, IEEE-CYBER 2015, June 9, 2015 - June 12, 2015, 2015: 1327-1332.

[12] Zong C-G, Gao X-S, Yu Y, et al. Kinematics analysis for obstacle-surmounting capability of a joint double-tracked robot[J]. Journal of Beijing Institute of Technology (English Edition), 2016, 25(2): 202-210.

[13] Hong S, Wu M, Xiao J, et al. Kylin: A transformable track-wheel hybrid robot[C]. 2017 International Conference on Advanced Mechatronic Systems, ICAMechS 2017, December 6, 2017 - December 9, 2017, 2018: 7-12

[14] Yuting Z, Baoling H, Qingsheng L, et al. Design and Implementation of Four-link Robot Crawler with Variable Structure[C]. 2018 3rd International Conference on Automation, Control and Robotics Engineering, CACRE 2018, July 19, 2018 - July 22, 2018, 2018.

[15] Zhu Y, Wang M, Li B, et al. Structure parameter optimization of a variable geometry tracked robot for structured environment[C]. 5th Annual IEEE International Conference on Cyber Technology in Automation, Control and Intelligent Systems, IEEE-CYBER 2015, June 9, 2015 - June 12, 2015, 2015: 1344-1349.

[16] Zou M, Bai H, Wang Y, et al. Mechanical design of a self-adaptive transformable tracked robot for cable tunnel inspection[C]. 13th IEEE International Conference on Mechatronics and Automation, IEEE ICMA 2016, August 7, 2016 - August 10, 2016, 2016: 1096-1100.

[17] Zou M, Bai H, Wang Y, et al. Mechanical design of a self-adaptive transformable tracked robot for cable tunnel inspection[C]// IEEE International Conference on Mechatronics and Automation. IEEE, 2016:1096-1100.

RESEARCHERID
THOMSON REUTERS

[Tang* *et al.,* 8(8): August, 2019]
IC™ Value: 3.00

ISSN: 2277-9655
Impact Factor: 5.164
CODEN: IJESS7

[18] Cui D, Gao X, Guo W, et al. Design and Stability Analysis of a Wheel-Track Robot[C]. 3rd International Conference on Information Science and Control Engineering, ICISCE 2016, July 8, 2016 - July 10, 2016, 2016: 918-922.

[19] Cui D, Guo W, Dong H, et al. The structure design and analysis of a wheel-track robot[C]. 13th IEEE International Conference on Mechatronics and Automation, IEEE ICMA 2016, August 7, 2016 - August 10, 2016, 2016: 2530-2535.

[20] Han Z, Xu X, Xu X, et al. Conceptual design of a wheel-track hybrid mobile robot[C]. 2018 IEEE/ASME International Conference on Advanced Intelligent Mechatronics, AIM 2018, July 9, 2018 - July 12, 2018, 2018: 664-669.

[21] Luo Z, Shang J, Wei G, et al. A reconfigurable hybrid wheel-track mobile robot based on Watt II six-bar linkage[J]. Mechanism and Machine Theory, 2018, 128: 16-32.

[22] Zhang M, Li M, Tian Y, et al. Design and kinematics analysis of single crawler wheel-track compound passive adaptive mobile robot[J]. Huazhong Keji Daxue Xuebao (Ziran Kexue Ban)/Journal of Huazhong University of Science and Technology (Natural Science Edition), 2018, 46(3): 69-74.

[23] Fujita T, Sasaki T. Development of hexapod tracked mobile robot and its hybrid locomotion with object-carrying[C]. 5th IEEE International Symposium on Robotics and Intelligent Sensors, IRIS 2017, October 5, 2017 - October 7, 2017, 2018: 69-73.

[24] Fujita T, Sasaki T, Tsuchiya Y. Hybrid motions by a quadruped tracked mobile robot[C]. IEEE International Symposium on Safety, Security, and Rescue Robotics, SSRR 2015, October 18, 2015 - October 20, 2015, 2015.

[25] Zhu Y, Fei Y, Xu H. Stability Analysis of a Wheel-Track-Leg Hybrid Mobile Robot[J]. Journal of Intelligent and Robotic Systems: Theory and Applications, 2018, 91(3-4): 515-528.